Batteries & Supercaps

Research Article
doi.org/10.1002/batt.202200443

Chemistry Europe
European Chemical Societies Publishing

www.batteries-supercaps.org

Special Collection

Degradation of Quinone-based Flow Battery Electrolytes: Effect of Functional Groups on the Reaction Mechanism**

S. Nandi,[a] L. E. de Sousa,[a] T. Vegge,[a] and P. de Silva*[a]

Organic redox flow batteries are a promising technology for grid-scale energy storage from renewable energy resources. However, the chemical instability of the organic electrolytes prohibits wide-scale commercial implementation as energy storage materials. Therefore, understanding their chemical degradation is essential to develop new and resilient electrolyte materials. In this article, we comparatively studied the chemical degradation pathways of 4,5-dihydroxybenzene-1,3-disulfonic acid (BQDS) and 3,6-dihydroxy-2,4-dimethylbenzenesulfonic acid (DHDMBS) employing potential energy surface exploration. Both the acid-catalyzed and base-catalyzed pathways have been considered. Density functional theory was used to compare the energetics of the reaction paths. The role of functional groups was investigated to get insight into why BQDS is prone to degradation and DHDMBS is much more stable. Furthermore, we studied the effect of the functional groups on the correlation of free energy of degradation and the reduction potential of the quinones.

Introduction

Global warming prompts us to urgently shift from the conventional to renewable energy resources such as wind and solar energy. The energy from solar and wind power is highly intermittent, and therefore, a grid-scale storage system is required. Redox flow batteries (RFB) are a promising technology that has the potential to become commercially available at a large scale to solve the grid-scale energy storage problem.[1] To date, most of the commercially available redox flow batteries use metal-ion-based electrolytes.[2–5] This makes the electrolytes environmentally harmful. Also, their scarcity and geopolitics sometimes make them commercially expensive. These shortcomings prompt the scientific community to look for alternative electrolytes for RFBs. Organic redox flow batteries (ORFBs) are one of the greener and cheaper alternatives for intermittent energy storage compared to metal-ion-based redox flow batteries.[6] The organic electrolytes, constituted of simple organic molecules, can be engineered to improve their physicochemical properties and be prepared from inexpensive raw materials.[7] However, chemical degradation of ORFB electrolytes, which leads to the loss of the desired electrochemical properties, imposes a major challenge for their commercial use.[8] Therefore, many researchers are actively trying to develop new molecules to improve their stability as RFB electrolytes.[9]

Among the organic molecules, quinones are one of the most studied electrolyte materials for ORFBs. Since their first utilization in this context,[10] the quinone-based electrolytes have gained attention for further research and development. The redox chemistry of quinones is generally well known, and their physicochemical properties can be tuned by changing functional groups. For example, Er et al. performed a computational high-throughput screening based on density functional theory by changing functional groups of various quinone skeletons to predict suitable electrolytes.[11] Such high-throughput studies can be used to discover new types of ORFB materials with higher efficiencies, which can be of great advantage for rapid development of new electrolytes.

Molecular engineering based on functional group tuning can lead to electrolytes with better electrochemical efficiencies. However, the molecular species may turn out to be chemically unstable. Chemical stability is very difficult to predict a priori. One way to include chemical stability in the high-throughput screening would be to incorporate the potential energy surface (PES) exploration tools into the screening procedure. However, this would make screening computationally very expensive. Alternatively, one could include the known degradation reactions that a target molecule might undergo into the screening procedure to account for at least some degradation pathways. Tabor et al. used computational screening, which considered chemical reactions to find correlations between the reduction potential and the ease of degradation for a library of quinones.[12] The screening study considered a few types of degradation reactions, namely 1,4 Michael addition (MA), gem-diol formation, and substitution reactions. However, the possibility of parasitic reactions involving the attached functional groups was not considered. Furthermore, the quinones are used at different pH values to control their redox potentials or chemical stability. This leads to a situation when the

[a] Dr. S. Nandi, Dr. L. E. de Sousa, Prof. T. Vegge, Prof. P. de Silva
Department of Energy Conversion and Storage,
Anker Engelunds Vej 301, 2800 Kongens Lyngby, Denmark
E-mail: pdes@dtu.dk

[**] A previous version of this manuscript has been deposited on a preprint server (https://doi.org/10.26434/chemrxiv-2022-f8j3l).

Supporting information for this article is available on the WWW under https://doi.org/10.1002/batt.202200443

Special Collection An invited contribution to a Special Collection dedicated to Aqueous Electrolyte Batteries.

Research Article
doi.org/10.1002/batt.202200443
Chemistry Europe
European Chemical Societies Publishing

degradation may either be catalyzed by an acid or a base. Although the end products of both the acid- and base-catalyzed degradation are same, their kinetics may vary. So, it is important to understand the chemical significance of the functional groups and analyze their effect on the mechanism for acid- and base-catalyzed reaction conditions.

4,5-dihydroxybenzene-1,3-disulfonic acid (BQDS) and 3,6-dihydroxy-2,4-dimethylbenzenesulfonic acid (DHDMBS) are two examples of organic molecules that have been proposed as ORFB electrolytes. BQDS was first shown to have the potential to be used as a posolyte in an all-organic aqueous flow battery.[10] However, it was later shown that BQDS undergoes Michael addition with H_2O and forms fully-substituted 1,2,4,6-tetrahydroxybenzene-3,5-disulfonic acid.[13] This degradation product leads to the loss of electrochemical efficiency and creates multiple technical problems.[14,15] Later, DHDMBS, a substituted para benzoquinone, was designed as a Michael-reaction-resilient ORFB electrolyte.[15] It was shown later that DHDMBS undergoes protodesulfonation reactions in acid media by a reaction mechanism that is reversed to sulfonation.[16] Nonetheless, the BQDS and DHDMBS constitute a perfect pair to study the effects of functional groups on different degradation mechanisms.

In this article, we study the effect of two functional groups, namely CH_3 and SO_3H, on the free energy of degradation by choosing BQDS and DHDMBS as a test case. Different possible degradation paths for 1,4 MA or similar types of reactions are studied. To understand the effects of the two functional groups, we systematically increase the complexity of the model systems by introducing the functional groups one by one to the simplest quinones. First, the effect of the functional groups is discussed in terms of the reaction free energies within the respective subsets. Then the degradation mechanism of BQDS and DHDMBS was compared between each other. Finally, we analyze the relationship between the reduction potentials of the quinones and their degradation reactions' free energies.

Computational Details

BQDS and DHDMBS differ in their backbone structures; BQDS is a substituted ortho-benzoquinone, and DHDMBS is a substituted para-benzoquinone. In accordance with this similarity, our model system consists of two subsets of quinones. Each of these subsets contains molecules that start at the benzoquinone and end in either BQDS or DHDMBS by gradually increasing the number of functional groups. The model systems studied here are pictorially represented in Scheme 2.

For constructing the reaction paths, both acid- and base-catalyzed reaction mechanisms were considered. The proton was modelled as solvated H_3O^+, H-bonded with three H_2O molecules (Figure 1a). Similarly, the OH^- anion was modeled as H-bonded to four H_2O molecules (Figure 1b). It was shown that these two models acurately represent the solvated proton and OH^-, and are prone to the least errors.[17–19] Correspondingly, the energies of the H_2O when required to balance out the elementary steps were chosen as tetramer or pentamers in their global minima geometries.[20] When required, the energy of a single H_2O molecule was derived from the energy difference between $(H_2O)5$ and $(H_2O)4$ (Figure 1c and d).

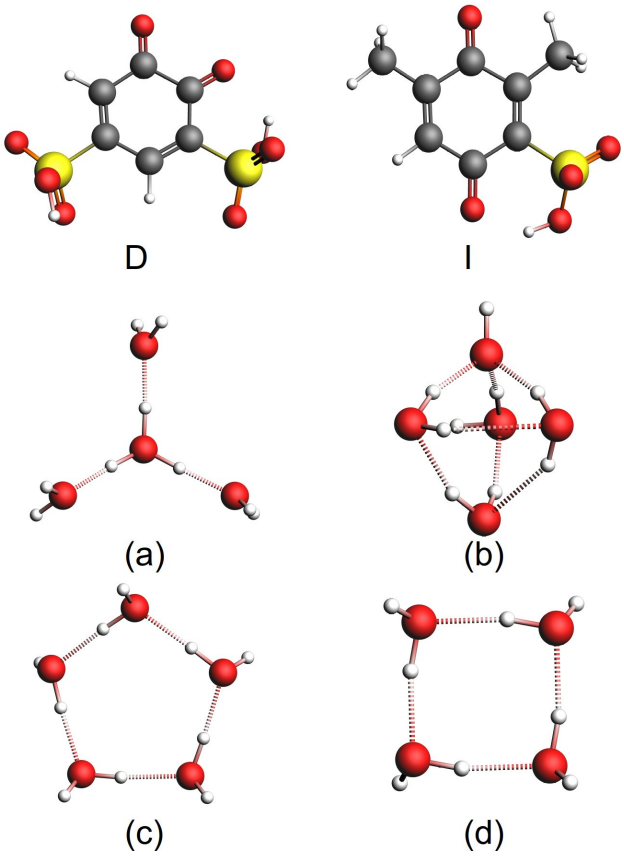

Figure 1. 3d models of **D**, **I**, a) $ceH_9O_4^+$, b) H_9O_5, c) $H_{10}O_5$, and d) H_8O_4.

Three main reaction steps were considered for the degradation paths in both acid and base medium. We arbitrarily assume the pH for the acidic medium to be 0.0 and for the basic medium to be 14.0. For the acid-catalyzed path, the reaction sequences are 1) protonation of the carbonyl group, 2) H_2O addition, and 3) aromatization. For the base-catalyzed reaction path, the reaction sequences are 1) OH^- addition, 2) aromatization by R_3 elimination as R_3OH, and 3) proton rearrangement according to the pK_a values of the product (Scheme 1). The acid-catalyzed reaction paths are based on the mechanism proposed in the literature.[21] The first protonation step facilitates the subsequent H_2O addition. The H_2O addition step in the acid medium is not a single elementary step even though in Scheme 1 it is presented as a single step. The H_2O addition follows proton transfer from the newly added H_2O to the unprotonated carbonyl group of the quinone. While sulfonic groups have negative pK_a values, we kept them protonated for the pH = 0 calculations. The reason was that we were not able to converge the calculations for some of the zwitterionic intermediates in the acid-catalyzed reactions, which most likely would require microsolvation to be stabilized. For the base-catalyzed path, all the SO_3H groups were deprotonated. Furthermore, for the base-catalyzed path, we considered up to two products' OH groups to be deprotonated according to their pK_a values (Table S2). In each of the cases, we considered the step with the highest energy as the thermodynamically limiting (TL) steps which controls the rate of the degradation path. The reaction free energy of the thermodynamically limiting step is denoted as ΔG_{TL}, and the reaction energy is denoted as ΔG_r. Figure 2 depicts the types of products considered in the study, with the quinone form of

Research Article
doi.org/10.1002/batt.202200443
Chemistry Europe
European Chemical Societies Publishing

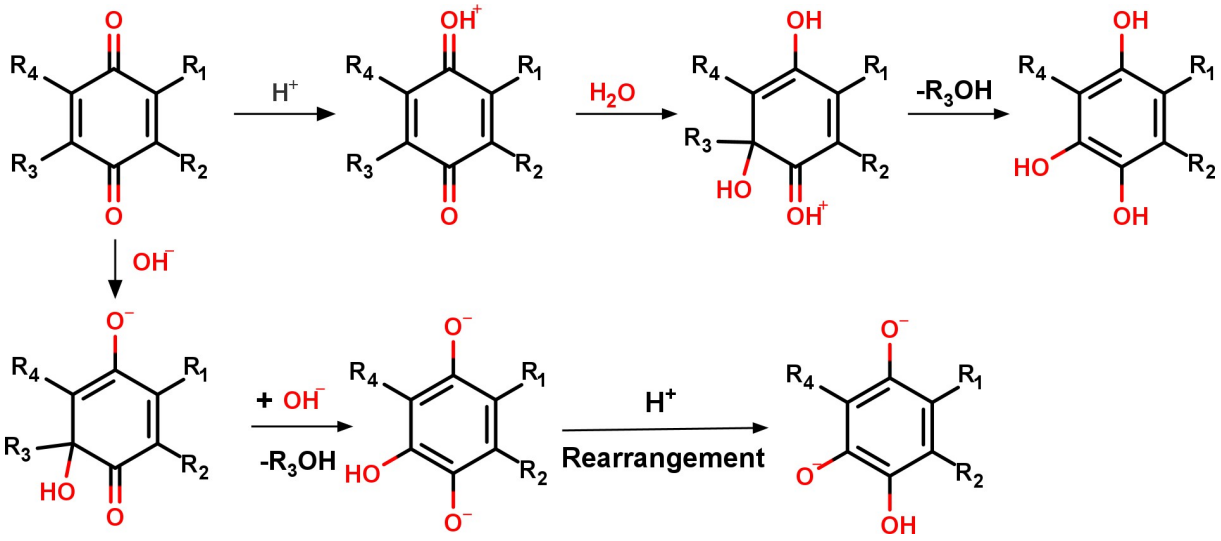

Scheme 1. The general steps considered for the acid and base-catalyzed pathways for all the degradation reactions. The last step for the base catalyzed path is dependent on the p*K*a of the protons.

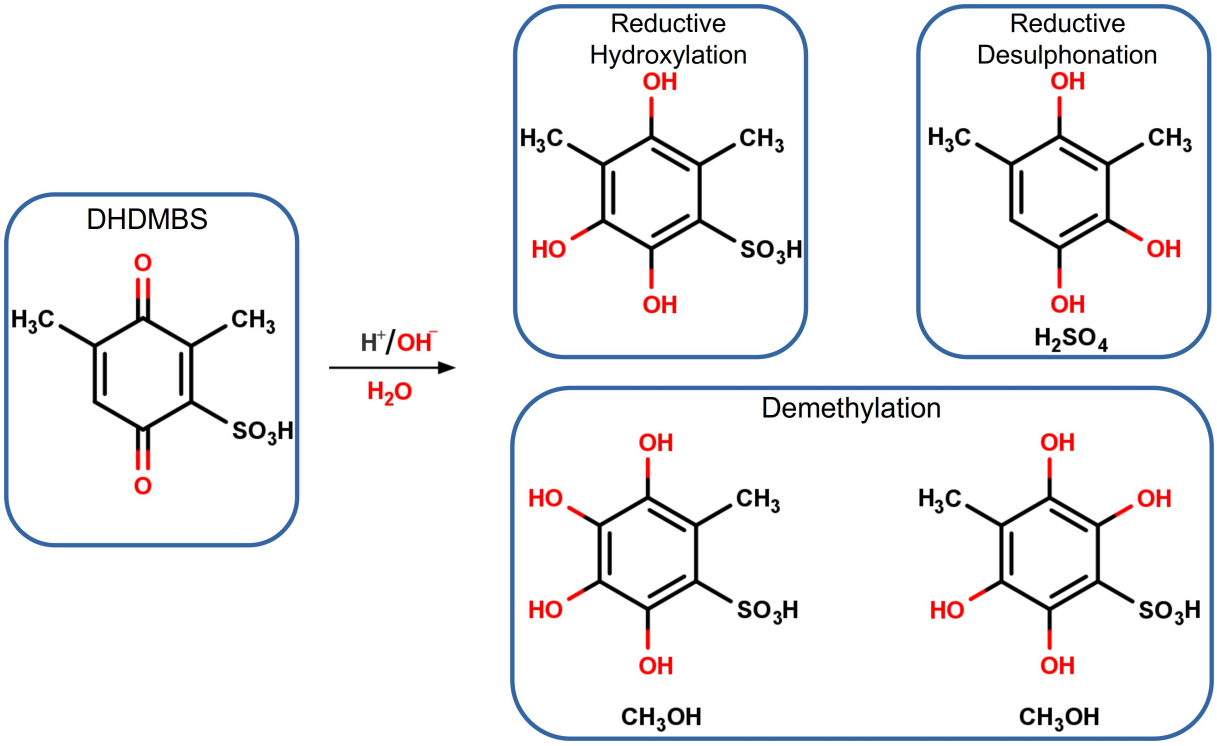

Figure 2. Depiction of different types of products formed by the chemical degradation with and without the involvement of the functional groups. The quinone form of the DHDMBS (I) is taken as an example.

DHDMBS as an example. For clarity, reductive hydroxylation indicates the addition of the OH group, reductive desulfonation indicates the removal of SO_3H group, and reductive demethylation indicates the removal of CH_3 as CH_3OH. For each case, the quinone gets reduced to the corresponding triol. In addition to these paths, the protodesulfonation path (Figure S17) is also considered.

Due to the flexible nature of the functional groups, many conformations are possible for the reactant, intermediate, and product geometries. Hence, before calculating the reaction energies, conformation search of each of the stationary points was performed. A stochastic algorithm was used to explore the potential energy surfaces and find different conformations corresponding to minima.[22,23] This algorithm uses the normal modes of the molecules to sample the conformational space. The detailed procedure is discussed in the Supporting Information.

All the species involved in the reaction paths were optimized using density functional theory (DFT). The B3LYP functional[24–26] was used to optimize the geometries. The conductor-like polarizable contin-

Research Article
doi.org/10.1002/batt.202200443
Chemistry Europe
European Chemical Societies Publishing

uum model (CPCM) with water as an implicit solvent was used to optimize the geometries. The redox potential of quinones calculated with B3LYP funtional and implicit solvation model was shown to match the experimental values quite well.[27] For the acid-catalyzed pathway, we used the 6-311G(2df,2p) basis set and for the base-catalyzed pathway, we added diffusion to the basis set (6-311++G(2df,2p)) to account for the negative charges. Grimme's D3 correction was used to account for the dispersion interaction.[28] The optimizations and single point calculations were carried out using Gaussian 16 software package.[29] The pK_a predictions were done using the ChemAxon software package which uses a cheminformatics based approach.[30]

We calculated the redox potentials of the quinones in both acid and base medium to compare with their reactivity. Quinones usually undergo a $2e^-/2H^+$ proton coupled electron transfer at low pH and $2e^-$ reduction at high pH. To compute the redox potential in the acidic medium, we used the reduction reaction:

$$\mathrm{Ox} + ne^- + n'\mathrm{H}^+ \rightarrow \mathrm{Red} \quad (1)$$

where, n is the number of electron, n' is the number of protons. Then, the standard redox potential is:

$$U^0 = -\frac{1}{ne}\Delta G^0_{\mathrm{sol}} - U_{\mathrm{SHE}} \quad (2)$$

where, e is the elementary charge. We used the value of U_{SHE} as 4.43 V.[31] The quantity $\Delta G^0_{\mathrm{sol}}$ can be expressed as:

$$\Delta G^0_{\mathrm{sol}} = G^0_{\mathrm{sol}}(\mathrm{Red}) - G^0_{\mathrm{sol}}(\mathrm{Ox}) + n'\Delta G^0_s(\mathrm{H}^+) \quad (3)$$

where, $G^0_{\mathrm{sol}}(\mathrm{Ox})$ and $G^0_{\mathrm{sol}}(\mathrm{Red})$ are the free energies of the oxidized and reduced species respectively in solvated condition. We used the value of $\Delta G^0_s(\mathrm{H}^+) = -11.38$ eV.[32] To compute the reduction potential in the basic medium, we simply put $n' = 0$ in the Equations (1) and (3). To calculate the reduction potential, we assumed that the SO_3H groups of the quinones remain fully protonated in acid medium and deprotonated in base medium.

Results and Discussion

ΔG_r of the reactions in acid are given in Table 1. In the case of the BQDS subset (**A**–**D**) (see Scheme 2), ΔG_r gradually decreases from −0.73 eV to −1.22 eV for the reductive hydroxylation pathway. Since one SO_3H group is added successively from **A** to **D**, this gradual decrease of ΔG_r implies that the SO_3H group facilitates degradation irrespective of their position and reaction paths. Similarly, ΔG_r for reductive desulfonation decreases from −0.91 eV to −1.28 eV from **B** to **D**. It is interesting to note that for **B** and **C**, which differ by only the position of the SO_3H group, the ΔG_r varies at most 0.13 eV for the acid-catalyzed degradation to hydroxylated products or desulfonated products. This indicates that the SO_3H group exerts very little effect due to positional isomerism on the free energy of degradation reaction of the quinones.

For the DHDMBS subset (Scheme 2), the effect of the SO_3H group on ease of acid-catalyzed degradation is also prominent and in this case ΔG_r decreases from **E** (−0.46 eV) to **F** (−0.68 eV). However, from **G** to **I**, for which a CH_3 group is added successively in addition to the SO_3H group, the ΔG_r increases from −0.59 to −0.34 eV for the reductive hydroxylation path. A similar trend is also observed for the reductive desulfonation path. The ΔG_r gradually increases from −0.68 eV in **F** to −0.40 eV in **I** with the introduction of CH_3 groups. The effect of the positional isomerism of the CH_3 group is not prominent for both the reductive hydroxylation and desulfonation paths. On a different note, the new CH_3 group opens up a possibility of reductive demethylation. The ΔG_r for demethylation is, however, very small for both **G** and **H**. The decrement of the exergonicity of the reductive dyhydroxylation by the CH_3 group indicates that it incorporates some inertness to the system for the acid-catalyzed pathway. The ΔG_r for the base-catalyzed path has quite different trend compared to the acid-catalyzed path. It increases only slightly from −0.36 eV to −0.27 eV for the hydroxylation path (from **A** to **D**). For the DHDMBS subset, there is no clear trend of the ΔG_r which can be attributed to either of the functional groups SO_3H, and CH_3.

Table 1. The reaction free energies (ΔG_r [eV]) and energy of the thermodynamically limiting steps (ΔG_{TL} [eV]) of the acid-catalyzed paths for the different types of degradation products, namely reductive hydroxylation, demethylation, and desulfonation. The 2D molecular geometries are provided in Scheme 2.

	OH		OS_3H		CH_3	
Molecule	ΔG_r	ΔG_{TL}	ΔG_r	ΔG_{TL}	ΔG_r	ΔG_{TL}
	BQDS					
A	−0.73	0.88	–	–	–	–
B	−0.93	1.06	−0.91	1.06	–	–
C	−1.06	0.97	−0.97	1.02	–	–
D	−1.22	1.34	−1.28	1.49	–	–
	DHDMBS					
E	−0.46	0.83	–	–	–	–
F	−0.68	1.16	−0.68	1.16	–	–
G	−0.59	1.18	−0.64	1.18	−0.06	1.18
H	−0.56	1.11	−0.53	1.17	−0.08	1.11
I	−0.34	1.24	−0.40	1.24	0.04	1.08

Research Article
doi.org/10.1002/batt.202200443
Chemistry Europe
European Chemical Societies Publishing

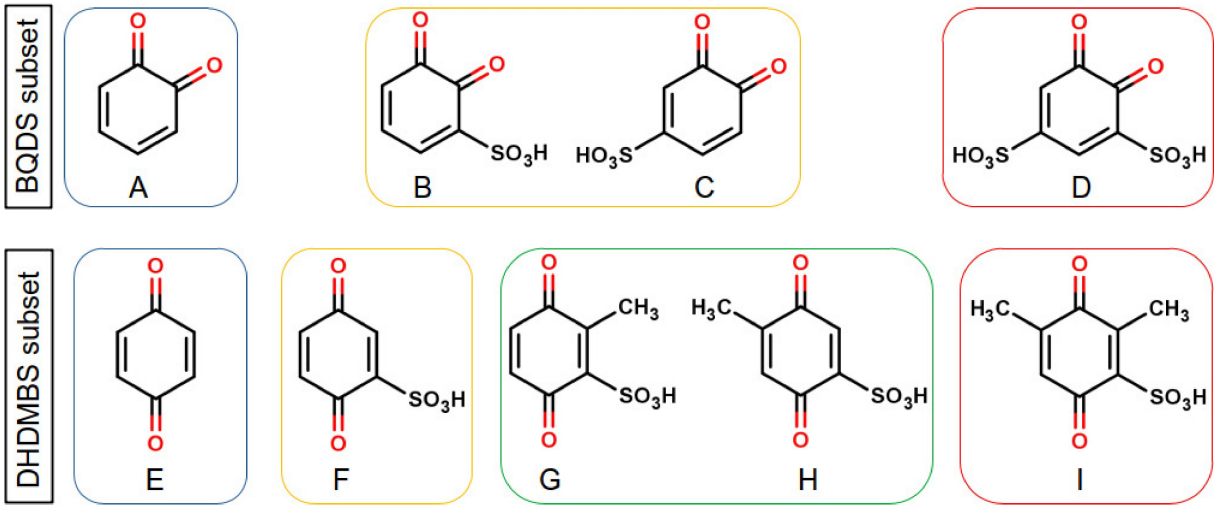

Scheme 2. The set of molecules investigated in this study. The colored box around the molecules indicates the similarity of the complexity of the molecules. The blue box indicates the unsubstituted quinones. The yellow box indicates the quinone with one SO_3H group. The red box indicates the quinone forms of BQDS (above) and DHDMBS (below).

The ΔG_r of the base-catalyzed reductive hydroxylation path for **I** is highly positive compared to the others and seem to be an outlier. For the reductive desulfonation path, the ΔG_r decreases only slightly for the BQDS subset (−0.49 eV to −0.55 eV). For the DHDMBS subset, the ΔG_r of reductive desulfonation are mostly negative except for **I** ($\Delta G_r = 0.19$ eV). Noticeably, the ΔG_r of the reductive demethylation for the base-catalyzed path are highly positive in contrast to the acid-catalyzed paths. Therefore, in terms of ΔG_r, the basic environment is more favourable than the acidic environment to suppress degradation.

In the literature, the formation of H_2SO_4 from **I** is attributed to protodesulfonation (**J**→**K**→**L**; Figure S17).[33] However, **L** can also be formed from the desulfonated product (**IPa1**) which we propose in this study (**I**→**IPa1**→**O**, Supporting Information). Interestingly, the ΔG_r for the pathway **I**→**IPa1**→**O** is −0.23 eV while that of the pathway **J**→**O** is −0.07 eV. Nevertheless, the formation of H_2SO_4 is a very probable degradation path for the sulfonated quinones.

ΔG_{TL} varies widely between the acid and base-catalyzed paths. For all the acid-catalyzed paths, the protonation step is the thermodynamically limiting step. For base-catalyzed path, the thermodynamically limiting step is mostly the OH^- addition step. Generally, the ΔG_{TL} of the acid-catalyzed paths, which is the protonation step, is much higher compared to that of the base-catalyzed reactions. This is expected as most of the quinones are electron deficient due to the presence of the SO_3H groups and thus addition of OH^- is more favourable than the addition of H_2O.

For the BQDS subset (**A**–**D**), the ΔG_{TL} for the acid-catalyzed reductive hydroxylation paths increases steadily from 0.88 eV to 1.34 eV with the increment of the SO_3H groups. The ΔG_{TL} for desulfonation path also increases from 1.06 eV for **B** to 1.49 eV for **D** (Table 1). For all the quinones in the BQDS subset, the reductive desulfonation is kinetically less favorable compared to reductive hydroxylation. Overall the trend for ΔG_{TL} shows that the SO_3H group has the effect of making the degradation reaction slower. The trend of ΔG_{TL} for the DHDMBS subset (**E**–**I**, Table 1) shows that the ΔG_{TL} for reductive hydroxylation and reductive desulfonation is the maximum for **I**. This trend is interesting as this implies that even the presence of CH_3 groups makes the acid-catalyzed degradation process slower even though the overall increase in ΔG_{TL} is lower compared to the BQDS subset.

For the base-catalyzed reaction paths, the ΔG_{TL} does not vary as drastically as the acid-catalyzed reaction paths (Table 2). Similarly, the ΔG_{TL} for the base-catalyzed reductive desulfonation pathway remain around 0.10 eV. Compared to the BQDS subset, ΔG_{TL} for both the reductive dehydroxylation and reductive desulfonation for the DHDMBS subset is much higher. For the reductive hydroxylation, the highest ΔG_{TL} is for **I** and the highest ΔG_{TL} value is for **H** for the reductive desulfonation reactions. Hence, no clear trend is attributable to the CH_3 group in case of base-catalyzed degradation.

From the discussion above, it is clear that the SO_3H group has much influence on the energetics of the degradation pathways in the acidic medium. In contrary, the SO_3H group has minimal effect on both ΔG_r and ΔG_{TL} in the basic medium. The position of SO_3H group does not influence the ΔG_r value to a great extent. From the analysis of the DHDMBS subset, it can be stated that the presence of two CH_3 groups greatly decreases the exergonicity of the degradation in acid medium. The CH_3 group can increase the ΔG_{TL} value for base-catalyzed degradation and thereby can make the degradation slower for the DHDMBS compared to BQDS.

We further analyzed the most favorable reductive hydroxylation and desulfonation pathways of BQDS and DHDMBS for the acid-catalyzed paths in Figure 3. The reductive hydroxylation of BQDS involves around four times lower ΔG_r than DHDMBS. The ΔG_r for the reductive desulfonation of BQDS is similarly three times lower than the ΔG_r for reductive

Research Article
doi.org/10.1002/batt.202200443
Chemistry Europe
European Chemical Societies Publishing

Table 2. The reaction free energies (ΔG_r [eV]), and the energy of the thermodynamically limiting steps (ΔG_{TL} [eV]) of the basecatalyzed paths for the types of degradation products, namely reductive hydroxylation, demethylation, and desulfonation. The 2D molecular geometries are provided in Scheme 2.

	OH		OS_3H		CH_3	
Molecule	ΔG_r	ΔG_{TL}	ΔG_r	ΔG_{TL}	ΔG_r	ΔG_{TL}
	BQDS					
A	−0.36	−0.11	–	–	–	–
B	−0.38	0.06	−0.49	0.11	–	–
C	−0.30	0.13	−0.46	0.12	–	–
D	−0.27	0.03	−0.55	0.10	–	–
	DHDMBS					
E	0.12	0.51	–	–	–	–
F	−0.15	0.33	−0.37	0.24	–	–
G	0.02	0.50	−0.35	0.23	0.74	0.47
H	−0.14	0.49	−0.14	0.39	0.58	0.69
I	0.30	0.60	0.19	0.29	0.62	0.29

desulfonation of DHDMBS. At the same time, ΔG_{TL} for BQDS is only slightly higher than for DHDMBS.

Finally, we also studied the correlation between the reduction potential and the free energy of the degradation reactions for all the quinones in both acid and base media. The redox potentials of the quinones are given in Table 3 and the redox reactions in acid and base medium are depicted in Figure 4. The Table also contains the experimental acid-medium redox potentials that we were able to find in the literature. The agreement with our calculations is rather good and does not exceed 0.2 V. For basic conditions, the accuracy is much lower due to the large errors of the implicit solvation model for anions, and we expect that the errors to exceed 0.5 V.[27] The reduction potential in the acid medium gradually increases from **A** to **D**. For the para-benzoquinones, first, the redox potential increases from **E** to **F** with the addition of a $-SO_3H$ group. The reduction potential then slightly decreases with the introduction of one $-CH_3$ group. It further reduces to 0.77 V and −1.13 V in acid and basic conditions respectively for **I** with the introduction of two CH_3 groups.

There is a linear correlation between reduction potential in acid medium and ΔG_r (Figure 5). For the BQDS subset, the ΔG_r decreases with the increase of the reduction potential. In other words, with each functionalization by the SO_3H group to the quinones, the reduction potential increases but the ΔG_r decreases. For the DHDMBS subset, the change in the reduction potential and ΔG_r follow an opposite trend. For the DHDMBS subset, the ΔG_r first decreases with the functionalization with the SO_3H group (**E**→**F**, Figure 5). However, with the introduction of the CH_3 group (**G**, **H**), the reduction potential decreases, and the ΔG_r increases. For **I**, the reduction potential is minimum while the ΔG_r is the highest. This trend is well-matched with the expectation from the experimental data in the sense that the CH_3 group makes the quinone molecule resilient for degradation through reductive hydroxylation. Similar correlation exists for the acid-catalysed desulfonation reactions (Figure 5b). Interestingly, the second SO_3H group results in a relatively high decrease of the ΔG_r for the BQDS subset at the cost of only marginally improving the reduction potential for the reductive desulfonation. ΔG_{TL} and the reduction potential increases with the introduction of an SO_3H group in acid medium for the BQDS subset (Figure 5c). Similarly, for the acid-catalysed reductive desulfonation, the ΔG_{TL} increases with the increase in the redox potential. This trend is opposite to the trend of ΔG_r vs reduction potential for the acid-catalysed reductive hydroxylation reaction for the BQDS subset. ΔG_{TL} remains mostly unaffected by the change in the reduction potential for the acid-catalyzed reductive hydroxylation and desulfonation paths for the DHDMBS subset.

In the base-catalyzed reactions, both ΔG_r and ΔG_{TL} changes very little compared to the base-catalysed reactions for the BQDS subset. Moreover, the reduction potential also does not vary much for the BQDS subset in the basic medium. This is reflected from the correlation plots (Figure 6a). The ΔG_r for both reductive hydroxylation and desulfonation increases with the decrease in the reduction potential in the basic medium for the DHDMBS subset. The ΔG_{TL} only slightly increases with the decrease in reduction potential for the DHDMBS subset. Therefore, there is very little correlation between the reduction potential and either ΔG_r or ΔG_{TL} under the base-catalyzed conditions.

Table 3. Calculated reduction potentials (V) in acidic ("Acid") and basic ("Base") and experimental values in acid ("Experiment"). The reference to the previously reported experimental reduction potentials are indicated as subscript.

Species	Experiment	Acid	Base
A	0.83[34]	0.95	−0.76
B	–	1.04	−0.74
C	–	1.10	−0.75
D	1.10[13]	1.13	−0.71
E	0.70[34]	0.81	−0.92
F	0.72[8]	0.92	−0.89
G	–	0.83	−1.05
H	–	0.87	−0.98
I	0.82[13]	0.77	−1.13

Research Article
doi.org/10.1002/batt.202200443
Chemistry Europe
European Chemical Societies Publishing

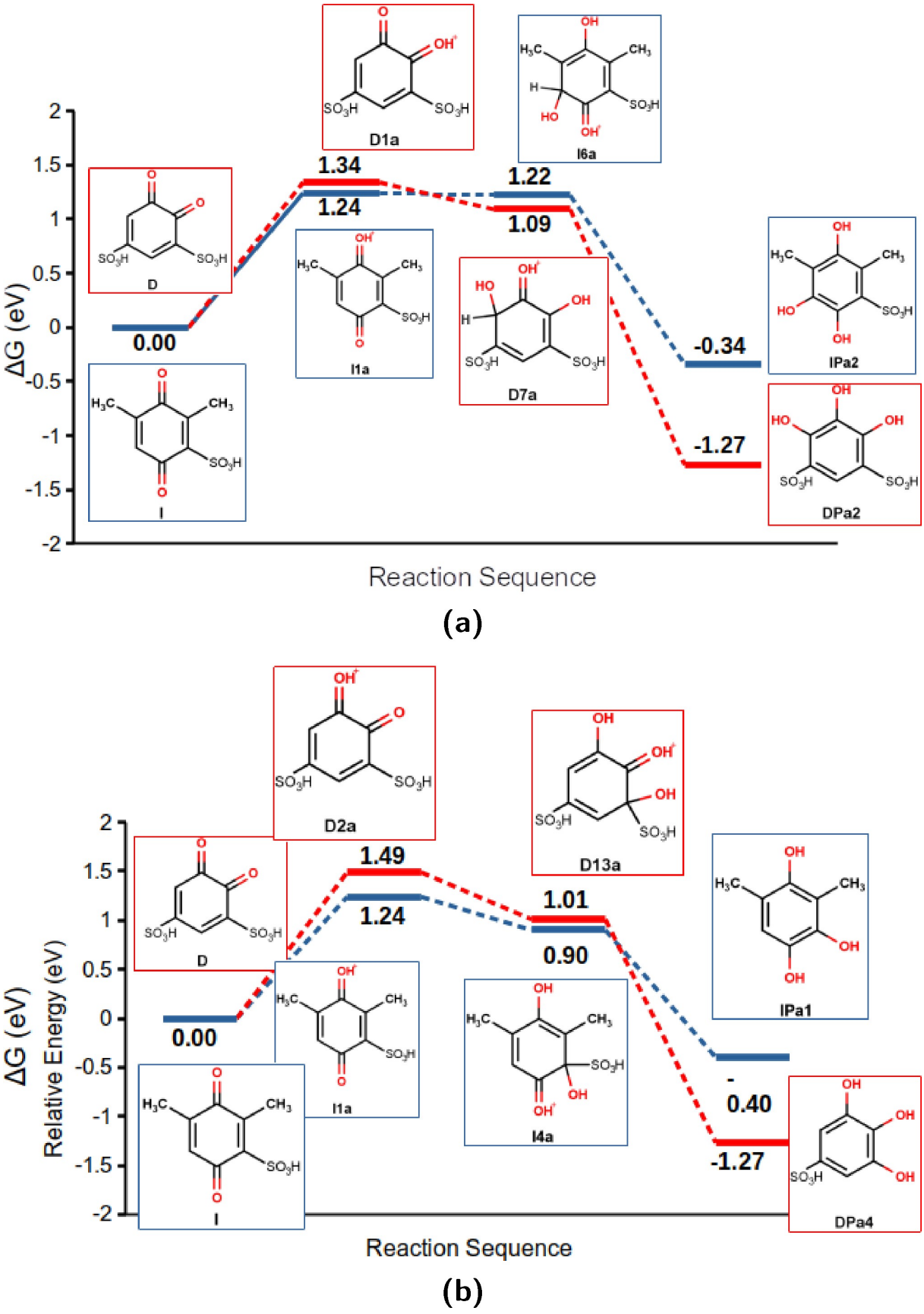

Figure 3. The relative energies vs reaction sequences for the energetically most favorable desulfonation and hydroxylation of D and I in acid. a) is the pathways that lead to a reductive dehydroxylated product, b) is the pathways that lead to reductive desulfonated product.

Research Article
doi.org/10.1002/batt.202200443
Chemistry Europe
European Chemical Societies Publishing

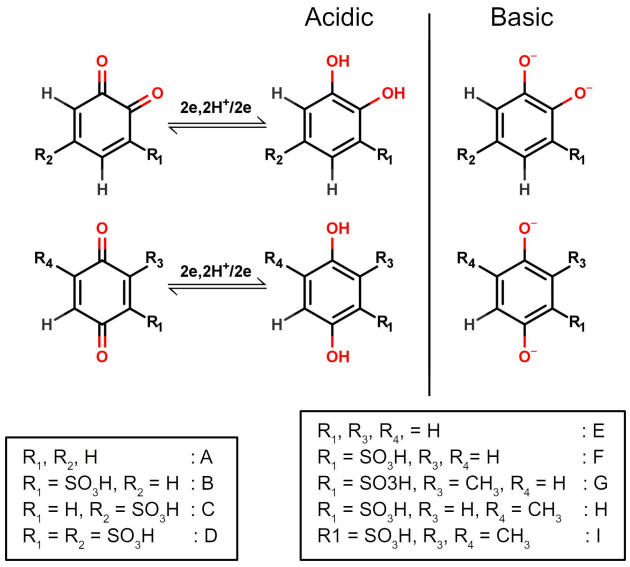

Figure 4. Schematic representation of the redox reaction for the quinones in acid and base medium.

Conclusion

In this paper, we studied the degradation mechanisms of BQDS and DHDMBS in acidic and basic environments. We built simplified model systems to understand the characteristic of the functional groups and their effect on degradation mechanisms and reduction potentials of the quinones. We found that the SO_3H group significantly influences the degradation either by taking part in the reaction mechanism or by decreasing the reaction free energy in acid medium. In contrast, the CH_3 group makes the quinones more inert by increasing the reaction free energy and sometimes by increasing the free energy of the thermodynamically limiting step in acid medium. In the base medium, the effect of these functional groups on the free energy changes are smaller than in acid medium. The nature of the quinones (ortho vs para) influences the reaction thermochemistry, and the para quinones are more stable compared to the ortho quinones, particularly in the base-catalyzed condition. We also provide an alternate reaction mechanism to the protodesulfonation as opposed to the published protodesulfonation path for H_2SO_4 formation in the case of DHDMBS. In any case, the relative ease of reductive desulfonation compared to the other degradation paths shows the importance of including

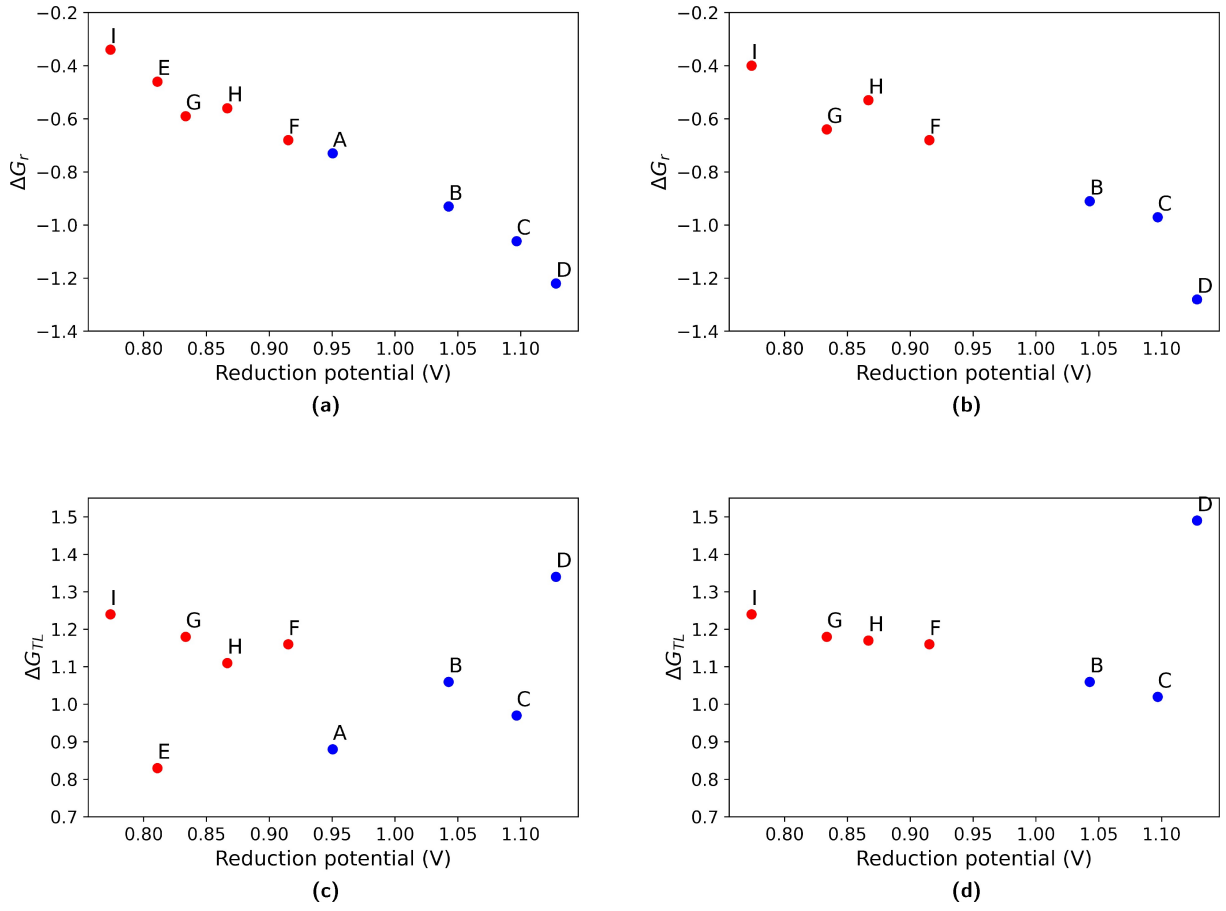

Figure 5. The correlation plot for the reduction potential (V) in acid medium vs the free energies of the acid-catalyzed degradation reactions: a) reduction potential vs ΔG_r for reductive hydroxylation, b) reduction potential vs ΔG_r for reductive desulfonation, c) reduction potential vs ΔG_{TL} for reductive hydroxylation, and d) reduction potential vs ΔG_{TL} for reductive desulfonation.

Research Article
doi.org/10.1002/batt.202200443
Chemistry Europe
European Chemical Societies Publishing

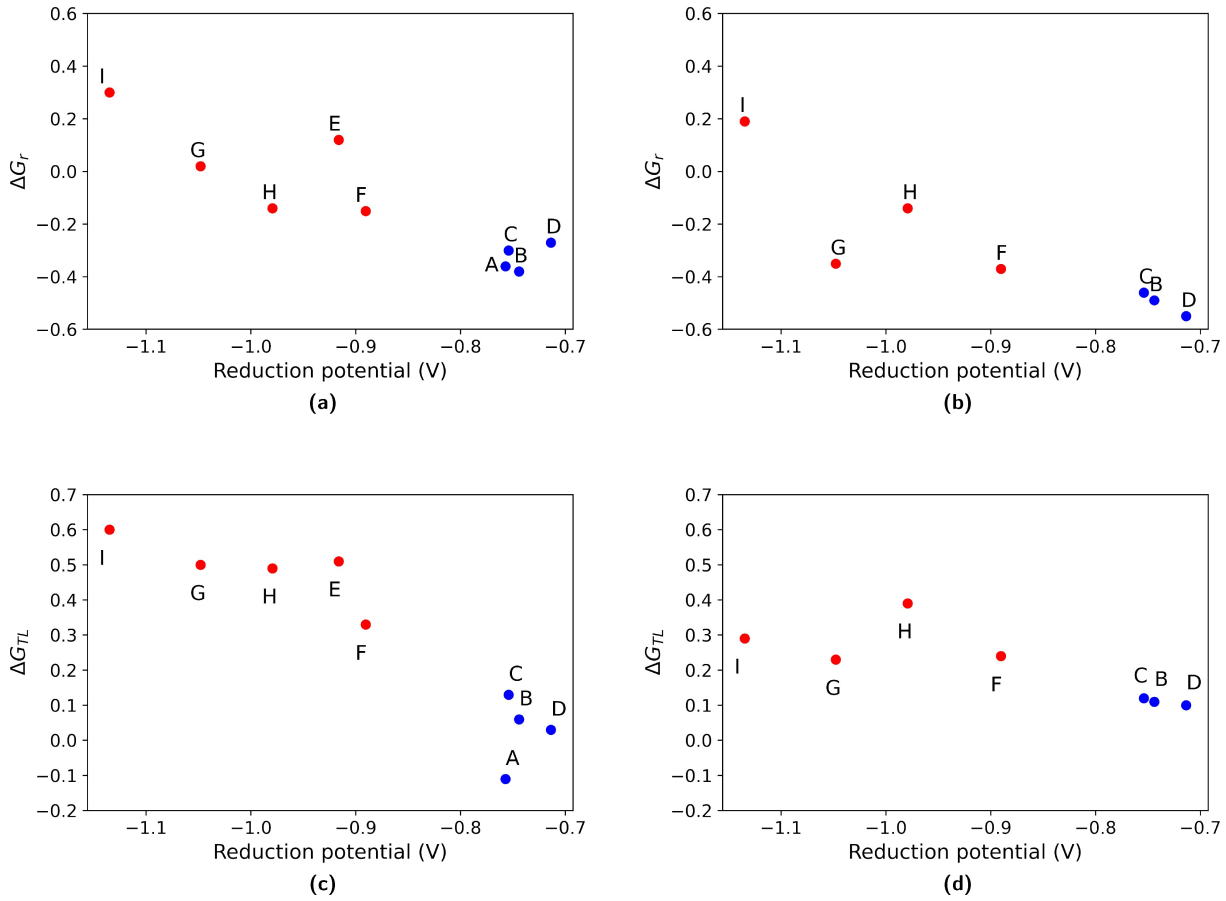

Figure 6. The correlation plot for the reduction potential (V) in base medium vs the free energies of the base-catalyzed degradation reactions: a) reduction potential vs ΔG_r for reductive hydroxylation, b) reduction potential vs ΔG_r for reductive desulfonation, c) reduction potential vs ΔG_{TL} for reductive hydroxylation, and d) reduction potential vs ΔG_{TL} for reductive desulfonation.

functional group reactivity in high-throughput screening approaches.

The reduction potential of the quinones exhibits an excellent correlation with the free energy for degradation in the acidic medium. This correlation is expected as both the degradation and the reduction of the quinones are reductive process. The correlation, implies that the SO_3H group helps increase the reduction potential at the cost of easier degradation. For the CH_3 group, the opposite is true. The introduction of two SO_3H group does not improve the reduction potential significantly but makes the quinone much more susceptible to the degradation.

Acknowledgement

The authors acknowledge support from the Novo Nordisk Foundation (SURE, NNF19OC0057822).

Conflict of Interest

The authors declare no conflict of interest.

Data Availability Statement

The data that support the findings of this study are available in the supplementary material of this article.

[1] Z. Zhu, T. Jiang, M. Ali, Y. Meng, Y. Jin, Y. Cui, W. Chen, *Chem. Rev.* **2022**, *0*, 10.1021/acs.chemrev.2c00289.
[2] K. Lourenssen, J. Williams, F. Ahmadpour, R. Clemmer, S. Tasnim, *J. Energy Storage* **2019**, *25*, 100844.
[3] L. H. Thaller, Electrically Rechargeable Redox Flow Cells, in *9th Intersociety Energy Conversion Engineering Conference* **1974**, p. 924–928.
[4] D. Pletcher, R. Wills, *Phys. Chem. Chem. Phys.* **2004**, *6*, 1779.
[5] M. Wu, T. Zhao, H. Jiang, Y. Zeng, Y. Ren, *J. Power Sources* **2017**, *355*, 62.
[6] J. Winsberg, T. Hagemann, T. Janoschka, M. D. Hager, U. S. Schubert, *Angew. Chem. Int. Ed.* **2017**, *56*, 686.
[7] R. P. Fornari, M. Mesta, J. Hjelm, T. Vegge, P. de Silva, *ACS Materials Lett.* **2020**, *2*, 239.
[8] K. Wedege, E. Dražević, D. Konya, A. Bentien, *Sci. Rep.* **2016**, *6*, 39101.
[9] D. G. Kwabi, Y. Ji, M. J. Aziz, *Chem. Rev.* **2020**, *120*, 6467.
[10] B. Yang, L. Hoober-Burkhardt, F. Wang, G. K. S. Prakash, S. R. Narayanan, *J. Electrochem. Soc.* **2014**, *161*, A1371.
[11] S. Er, C. Suh, M. P. Marshak, A. Aspuru-Guzik, *Chem. Sci.* **2015**, *6*, 885.
[12] D. P. Tabor, R. Gómez-Bombarelli, L. Tong, R. G. Gordon, M. J. Aziz, A. Aspuru-Guzik, *J. Mater. Chem. A* **2019**, *7*, 12833.
[13] B. Yang, L. Hoober-Burkhardt, S. Krishnamoorthy, A. Murali, G. K. S. Prakash, S. R. Narayanan, *J. Electrochem. Soc.* **2016**, *163*, A1442.
[14] J. B. Conant, L. F. Fieser, *J. Am. Chem. Soc.* **1924**, *46*, 1858.

[15] L. Hoober-Burkhardt, S. Krishnamoorthy, B. Yang, A. Murali, A. Nirmalchandar, G. K. S. Prakash, S. R. Narayanan, *J. Electrochem. Soc.* **2017**, *164*, A600.
[16] A. Murali, A. Nirmalchandar, S. Krishnamoorthy, L. Hoober-Burkhardt, B. Yang, G. Soloveichik, G. K. S. Prakash, S. R. Narayanan, *J. Electrochem. Soc.* **2018**, *165*, A1193.
[17] M. Śmiechowski, J. Stangret, *J. Chem. Phys.* **2006**, *125*, 204508.
[18] Y. Zeng, A. Li, T. Yan, *J. Phys. Chem. B* **2020**, *124*, 1817.
[19] R. Roszak, R. W. Góra, S. Roszak, *Int. J. Quantum Chem.* **2012**, *112*, 3046.
[20] J. Niesse, H. Mayne, *J. Comput. Chem.* **1997**, *18*, 1233.
[21] V. Krishnamurti, B. Yang, A. Murali, S. Patil, G. Surya Prakash, S. Narayan, *Curr. Opin. Electrochem.* **2022**, *35*, 101100.
[22] LeoX – Light Emission and Exciton Diffusion in Organic Molecules 0.4.0 **2022-03-15**, https://github.com/LeonardoESousa/LeoX.
[23] L. E. de Sousa, F. T. Bueno, G. M. de Silva, D. A. da Silva Filho, P. H. de Oliveira Neto, *J. Mater. Chem. C* **2019**, *7*, 4066.
[24] C. Lee, W. Yang, R. G. Parr, *Phys. Rev. B* **1988**, *37*, 785.
[25] A. D. Becke, *J. Chem. Phys.* **1993**, *98*, 5648.
[26] P. J. Stephens, F. J. Devlin, C. F. Chabalowski, M. J. Frisch, *J. Phys. Chem.* **1994**, *98*, 11623.
[27] R. P. Fornari, P. de Silva, *Molecules* **2021**, *26*, 3978.
[28] S. Grimme, J. Antony, S. Ehrlich, H. Krieg, *J. Chem. Phys.* **2010**, *132*, 154104.
[29] M. J. Frisch, G. W. Trucks, H. B. Schlegel, G. E. Scuseria, M. A. Robb, J. R. Cheeseman, G. Scalmani, V. Barone, G. A. Petersson, H. Nakatsuji, X. Li, M. Caricato, A. V. Marenich, J. Bloino, B. G. Janesko, R. Gomperts, B. Mennucci, H. P. Hratchian, J. V. Ortiz, A. F. Izmaylov, J. L. Sonnenberg, D. Williams-Young, F. Ding, F. Lipparini, F. Egidi, J. Goings, B. Peng, A. Petrone, T. Henderson, D. Ranasinghe, V. G. Zakrzewski, J. Gao, N. Rega, G. Zheng, W. Liang, M. Hada, M. Ehara, K. Toyota, R. Fukuda, J. Hasegawa, M. Ishida, T. Nakajima, Y. Honda, O. Kitao, H. Nakai, T. Vreven, K. Throssell, J. A. Montgomery, Jr., J. E. Peralta, F. Ogliaro, M. J. Bearpark, J. J. Heyd, E. N. Brothers, K. N. Kudin, V. N. Staroverov, T. A. Keith, R. Kobayashi, J. Normand, K. Raghavachari, A. P. Rendell, J. C. Burant, S. S. Iyengar, J. Tomasi, M. Cossi, J. M. Millam, M. Klene, C. Adamo, R. Cammi, J. W. Ochterski, R. L. Martin, K. Morokuma, O. Farkas, J. B. Foresman, D. J. Fox, Gaussian16 Revision C.01 **2016**, gaussian Inc. Wallingford CT.
[30] Marvin 21.3.0 **2021–10-06**, http://www.chemaxon.com/.
[31] H. Reiss, A. Heller, *J. Phys. Chem.* **1985**, *89*, 4207.
[32] C.-G. Zhan, D. A. Dixon, *J. Phys. Chem. A* **2001**, *105*, 11534.
[33] Y. Liu, Q. Chen, X. Zhang, J. Ran, X. Han, Z. Yang, T. Xu, *Curr. Opin. Electrochem.* **2022**, *32*, 100895.
[34] J. R. T. Johnsson Wass, E. Ahlberg, I. Panas, D. J. Schiffrin, *J. Phys. Chem. A* **2006**, *110*, 2005.

Manuscript received: October 5, 2022
Revised manuscript received: November 2, 2022
Accepted manuscript online: November 3, 2022
Version of record online: December 7, 2022